Article ID:#19610854. Received: August 31, 2021. Revised: September 10, 2021. Accepted: December 21, 2021

Journal of Information and Communication Engineering (JICE), 7 (2): 467-473, December 31, 2021
e-ISSN: 2432-5465, p-ISSN: 2186-9162
Applied Science and Computer Science Publications

Gastric Cancer Detection by Two-step Learning in Near-Infrared Hyperspectral Imaging

Ayano Yahata [1], Hiroshi Takemura [1], Ren Iwanami [2], Masakazu Umezawa [2], Kyohei Okubo [2], Kohei Soga [2], Toshihiro Takamatsu [3], Tomohiro Mitsui [4], Tomohiro Kadota [4], Takeshi Kuwata [4], Hiroaki Ikematsu [4] and Hideo Yokota [5]

Department of Mechanical Engineering, Tokyo University of Science, Noda, Chiba, Japan [1]
Email: 7520575@ed.tus.ac.jp

Department of Materials Science and Technology, Tokyo University of Science, Katsushika, Tokyo, Japan [2]

Research Institute for Biomedical Sciences, Tokyo University of Science, Noda, Chiba, Japan [3]

National Cancer Center Hospital East Kashiwa, Chiba, Japan [4]

RIKEN Center for Advanced Photonics, Wako, Saitama, Japan [5]

Abstract: Gastric cancer is one of the most serious cancers that affects and kills many people around the world every year. Early treatment of gastric cancer dramatically improves the survival rate. Endoscopy has become an important tool for early detection. Since invasive gastric cancer or the edge of the invasive gastric cancer is difficult to find by using conventional visible-light endoscopy, near-infrared imaging, which is bringing great progress to the medical field, is focused on in recent years. In order to apply near-infrared hyperspectral imaging (NIR-HSI) in real-time, wavelength feature extraction is important because a large amount of data needs to be analyzed. The purpose of this study is to detect gastric cancer using NIR-HSI and to select a suitable wavelength for the target in the near-infrared region (1000‑1600 nm). NIR-HSI was used to take data from six specimens of gastric cancer and each pixel was labeled as normal or tumor on the hyperspectral image based on the histopathological diagnosis. 4 wavelengths were extracted from 95 wavelengths using the least absolute shrinkage and selection operator method. Supervised learning was performed using a support vector machine for both cases using all 95 wavelengths and the case using 4 selected wavelengths. In both cases, the approximate location of the tumor could be identified, indicating that an appropriate wavelength could be selected. We were also able to improve the detection accuracy by creating new supervised data and adding another learner. The detection accuracy was 93.3% for accuracy, 69.8% for sensitivity, and 96.7% for specificity. These results show that gastric cancer can be detected even at four wavelengths. By applying the results of this study to the endoscope system, the possibility of constructing a NIR endoscope system for gastric cancer was suggested.

Keywords: Cancer detection; Gastric cancer; Near-infrared hyperspectral imaging; The least absolute shrinkage and selection operator; Support vector machine

I. INTRODUCTION

Gastric cancer remains serious cancer worldwide and is responsible for over one million new cases in 2020 and an estimated 769,000 deaths [1]. When gastric cancer is detected and treated at an early stage, the five-year survival rate can reach 90% [2, 3]. Endoscopy has become an important tool for cancer detection. However, invasive gastric cancer and its edge are hard to find even for experienced endoscopists since there is usually a lack of obvious gross morphological changes to be visualized under conventional visible-light endoscopy [4].

The near-infrared (NIR) region (1000‑2000 nm, also known as NIR-II/-III or second biological window [5]) offers high transparency in biological tissue. The NIR

Corresponding Author: Ayano Yahata. Department of Mechanical Engineering, Tokyo University of Science, Noda, Chiba, Japan, 7520575@ed.tus.ac.jp

light enables to probe the deep part of the living body [6]. Hyperspectral imaging (HSI) simultaneously acquires both spatial (localization) and spectral (identification) information [7] and is leading to emerging medical applications such as early detection of various types of cancer [8, 9]. Use of the NIR light for HSI vastly improves the applicability of this technology for practical case. Akbari et al. performed a study to identify gastric tumors using NIR-HSI. They have shown that it is possible to identify gastric cancer using a hyperspectral system that can acquired 239 wavelengths in the NIR region (1000-2500 nm) [10]. Sato et al. applied the NIR-HSI for the distinction of surgically resected gastrointestinal stromal tumor and showed that NIR light in the range of 1000-1600 nm was effective [11].

To apply NIR-HSI to real-time imaging, the number of wavelengths needs to be reduced for rapidly processing HSI data. In addition, the combination of wavelengths should be properly chosen depending on the optical properties, including absorption and scattering, of the target. Akimoto et al. reported the wavelength bands reduction method in NIR-HSI based on a deep neural network for tumor lesion classification [12].

The purpose of this study is to detect gastric cancer using NIR-HSI and to select a suitable wavelength for the target in the NIR region (1000-1600 nm). NIR-HSI was used to take data from six specimens of gastric cancer and each pixel was labeled as normal or tumor on the hyperspectral image based on histopathological diagnosis. To reduce the dimension of the hyperspectral image, the least absolute shrinkage and selection operator (LASSO) was employed. Supervised learning was performed using support vector machine (SVM) for both case using all wavelengths and the case using selected wavelengths.

II. METHODOLOGY

A. NIR-HSI System

In this study, the NIR composition imaging system (Compovision, CV-N800HS; Sumitomo Electric Industries, Ltd.) was used. The imaging system consists of a camera with a two-dimensional photodetector and a spectroscope for receiving NIR light (900-2400 nm). The composition and concentration distribution of substances can be measured in real time, non-destructively and non-contact, by irradiating NIR light on the target (Fig. 1).

B. Data Acquisition

We obtained data of six stomachs removed after diagnosis of gastric cancer. The border between the cancer and normal tissue was diagnosed by histopathological examination. All specimens were placed on a scanning table with the mucous membrane surface on top. Two-dimensional images were acquired by moving the scanning table on which the specimen was captured one line at a time (line scan), and then arranged the lines.

Fig. 2 shows an example of NIR image and spectral data (reflectance) at a pixel. The NIR image is a pseudo-

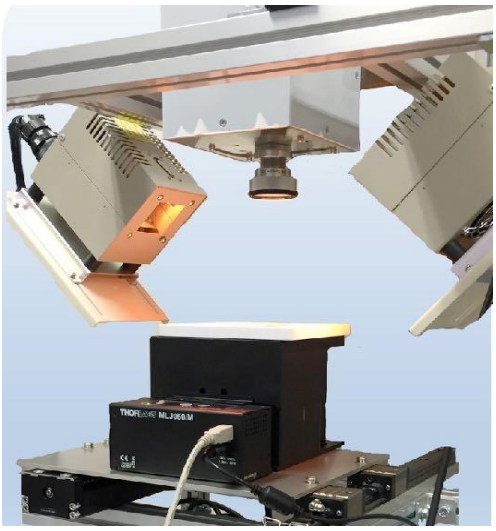

Fig. 1 NIR-HSI system.

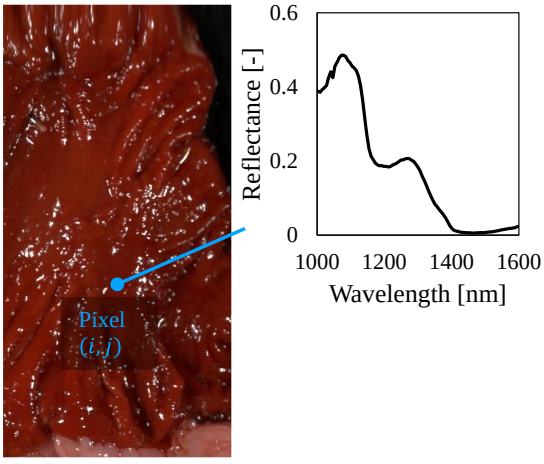

Fig. 2 An example of NIR pseudo-image and hyperspectral data including spectral and spatial dimensions obtained by Compovision. Reflectance of the pixel (i, j) (blue dot).

image in which the channels for 1091, 1211, and 1318 nm are assigned to red, green, and blue, respectively. The imaging system obtains three types of data: raw data (direct output from the camera); correction data (white data), which is acquired using a material that has no absorption in the entire NIR range; and correction data (dark data), which is acquired while the camera is shielded from light.

C. Normalization

The white data was used to correct for the wavelength sensitivity characteristics of the camera and light source, and the dark data was used to correct for the zero level. The reflectance of the pixel (i, j) was obtained by Equation 1.

$$R(i,j) = \frac{I_{\text{raw}}(i,j) - I_{\text{dark}}(i,j)}{I_{\text{white}}(i,j) - I_{\text{dark}}(i,j)} \quad (1)$$

I_{raw}: value of measured data, I_{dark}: value of dark data, I_{white}: value of white data. If the denominator is less than or equal to 0, the calculated value is set to 0.

D. Supervised data Creation

The wavelength range used was 1000–1600 nm (95 wavelengths). Wavelengths above 1600 nm were excluded from the analysis because of the low sensitivity of the NIR camera and the large absorption by water. The supervised data of the boundary between cancer and normal tissue was determined based on histopathological diagnosis. The specimens included normal tissue, exposed tumor tissue, unexposed tumor tissue, and necrotic tumor tissue. The NIR images annotated with them are shown in the leftmost column of Fig. 5. In the annotated NIR image, the red line represents the boundary of the exposed tumor tissue, the white line represents the boundary of the unexposed tumor tissue, and the yellow line represents the boundary of the necrotic tumor tissue.

In this study, we labeled normal tissue as normal and exposed tumor tissue as tumor for each pixel and obtained 788,527 data for normal and 105,623 data for tumor. The created supervised image is shown in the second column from the left in Fig. 5. In the supervised image, the green area represents "normal", and the red area represents "tumor".

E. Spectrum Extraction

Since hyperspectral images have large amounts of data containing spatial and spectral information, dimensionality reduction is one of the most important steps during the spectral analysis. To reduce the wavelengths of the hyperspectral data, LASSO was employed. LASSO was proposed by Tibshirani to simultaneously perform parameter estimation and variable selection in regression analysis [14]. The explanatory variables are reduced by linear regression so that equation 2 becomes smaller. The first term is the same equation as in the least-squares method, and variable selection is performed by setting the coefficient of the explanatory variable to zero in the second term.

$$\sum_{i=1}^{n}(y_i - \hat{y}_i)^2 + \lambda \sum_{j=1}^{m}|\beta_j| \quad (2)$$

n: Number of data, m: Number of explanatory variables, y: Objective variable, $\hat{y}$: Actual objective variable, β: Regression coefficients, and λ: parameter. LASSO performs better in feature selection than other methods such as Ordinary Least Square regression and Ridge Regression [15]. In this study, wavelength was the explanatory variable, and LASSO chose 4 wavelengths.

F. Classification

In hyperspectral data classification, several studies have shown the effectiveness of SVM in analyzing hyperspectral data [10, 15, 16]. SVM is a supervised classification method with excellent generalization capability, dealing with both linear and nonlinear data efficiently [17]. In this study, SVM was employed to identify tumors, and the kernel function was chosen as radial basis function (RBF). We applied leave-one-out cross-validation to the specimens, learning and classifying so that all specimens was test cases.

The performances of SVM models were evaluated by classification accuracy. The accuracy was evaluated by classifying the pixels into four groups (Table 1): tumor classified as tumor (true-positive: TP), tumor classified as normal (false-negative: FN), normal classified as tumor (false-positive: FP), and normal classified as normal (true-negative: TN). Based on these indicators,

Table 1 A matrix summarizing the results of the classifications output by binary classification.

		classification	
		tumor	normal
supervised	tumor	True Positive (TP)	False Negative (FN)
	normal	False Positive (FP)	True Negative (TN)

the accuracy (Equation 3), sensitivity (Equation 4), and specificity (Equation 5) were calculated. Since cancer is a lesion that should not be missed, sensitivity was used as the index for evaluation.

$$Accuracy\ [\%] = \frac{TP + TN}{TP + TN + FP + FN} \times 100 \quad (3)$$

$$Sensitivity\ [\%] = \frac{TP}{TP + FN} \times 100 \quad (4)$$

$$Specificity\ [\%] = \frac{TN}{TN + FP} \times 100 \quad (5)$$

G. Two-step Learning Machine

Using sensitivity to test the performance of the model results in false positives that classify "normal" as "tumor". Therefore, we proposed a two-stage learning method as shown in Fig. 3. After the machine learning by SVM, we labeled the data classified as "tumor" based on the pathological diagnosis as we did in the supervised data creation (the third row from the left in Fig. 6). The learner is the same SVM as described above. Leave-one-out cross-validation was performed, and Accuracy, Sensitivity, and Specificity were calculated.

III. RESULTS AND DISCUSSION

Fig. 4 shows the results of NIR-HSI extraction of normal and tumor from the data obtained from six specimens, and the average reflectance of each. The 4 wavelengths selected by LASSO were 1091, 1217, 1287, and 1400 nm. The results of classification for all 95 wavelengths and for 4 wavelengths are shown in Table 2.

Table 2 shows that even with 4 wavelengths, the classification was as good as when all 95 wavelengths were used, and at the same time, the optimal wavelength was selected. By using the optimal wavelength as the input feature, it was suggested that the system could be applied to real-time diagnosis with sufficient system.

The results of all the classification for each specimen by using the leave-one-out cross-validation are shown in Fig. 5. Although the approximate location of the tumor tissue was classified, the folds tended to be classified as the tumor, regardless of the number of wavelengths.

The tumor region has finer irregularities than the normal region, which makes it difficult for light to be reflected. Fig. 4 also shows that the overall reflectance of the tumor is lower than that of normal, suggesting that the tumor tissue has irregularities that easily scatter light.

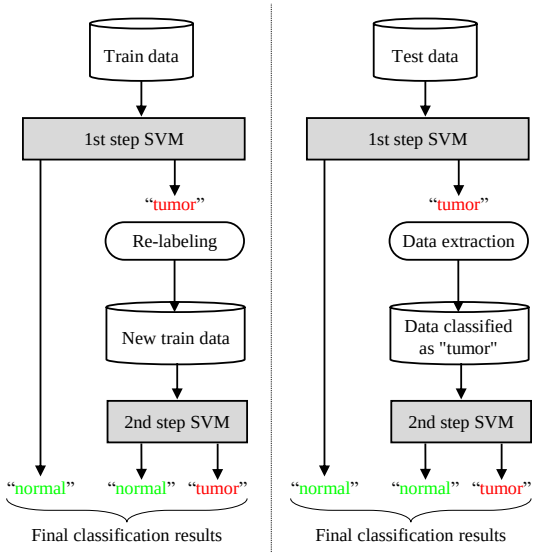

Fig. 3 Diagrams of learning and classification process. The left side shows the learning process using the two-stage learner. The data classified as "tumor" by the 1st step learner was re-labeled in the same way as the method for supervised data creation described above. The right side shows the classification by the two-step learner.
The data classified as "tumor" by the 1st step learner was reclassified by the 2nd step learner.

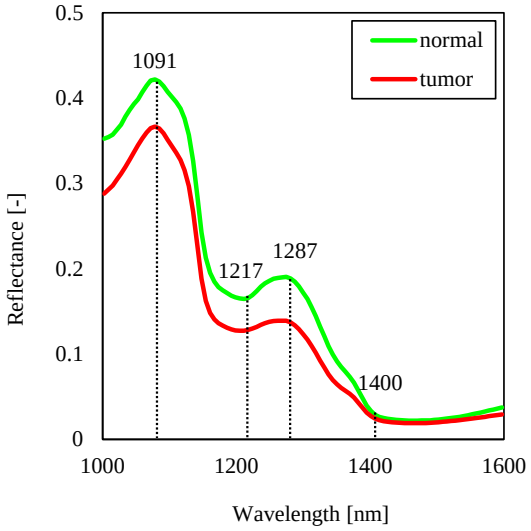

Fig. 4 The average spectrum of the reflectance of pixels in the normal and tumor regions. LASSO has selected 4 wavelengths: 1091, 1217, 1287, and 1400nm.

As a result, the light does not reflect well in the folds, and the classification results are likely to be false positives. Looking at the difference in classification results by the number of wavelengths, 4 wavelengths tended to classify more folds as false positives. It is thought that the 4 wavelengths were chosen since the normal region is less reflective than the tumor region. The classification results showed that the folds of the specimens tended to be classified as false positives, and this tendency became stronger when the wavelength was selected.

Table 3 and Fig. 6 show the results of two-step learning for the classification results of four wavelengths together with the results of one-step learning. From Fig. 6, the false positive was reduced because the folds that were falsely detected as "tumor" were detected more correctly than in the case of one-step learner. Specificity is an index that becomes 100% if all are classified as cancer, so it was low in two-step learning that was no longer classified as exaggerated. On the other hand, the accuracy and specificity have improved, and it can be said that the classification accuracy has improved. This is probably because the 1st step learning machine was able to classify normal tissue and tumor tissue and folds that do not reflect light well, and the 2nd step learning machine was able to classify tumor tissue and folds.

Some specimens were classified to be as large as the tumor region, while others were exaggeratedly classified to be tumor region. It is also possible that individual differences such as tumor size and contrast are preventing uniformity. Increasing the number of specimens could have prevented the poor discriminative ability of some specimens.

IV. CONCLUSION

In this study, NIR-HSI was used to detect gastric cancer on six specimens. Datasets of normal and tumor pixels were created from the hyperspectral images and classified using SVM. Comparing the results of using all 95 wavelengths and the 4 wavelengths selected by LASSO, we found that we could classify the data without loss of accuracy and selected optimal wavelengths. In addition, we were able to reduce the number of false positives and improve the classification accuracy by using two-stage learning. By applying the results of this study to the endoscopic system, the possibility of constructing a NIR endoscope system for gastric cancer was suggested.

We were able to show that we could non-invasive detect gastric cancer even with a reduced number of wavelengths. Our future work is to create a learning

Table 2 The results of classification for all 95 wavelengths and for 4 wavelengths.

	95 wavelengths	4 wavelengths
Accuracy [%]	82.2	82.3
Sensitivity [%]	93.0	96.8
Specificity [%]	80.8	82.7

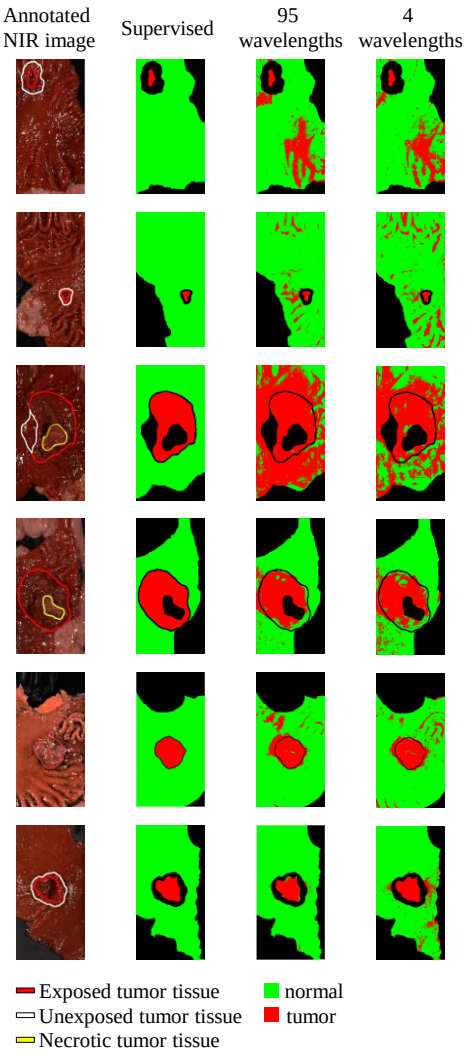

Fig. 3 Summary of images for comparison between the case using all 95 wavelengths and the case using 4 selected wavelengths. From left to right: annotated NIR image, supervised image, results of classification at all 95 wavelengths, and results of classification at 4 selected wavelengths.

Table 3 The result of classification by two-step learner.

	One-step learner	Two-step learner
Accuracy [%]	82.3	92.6
Sensitivity [%]	96.8	68.1
Specificity [%]	82.7	96.7

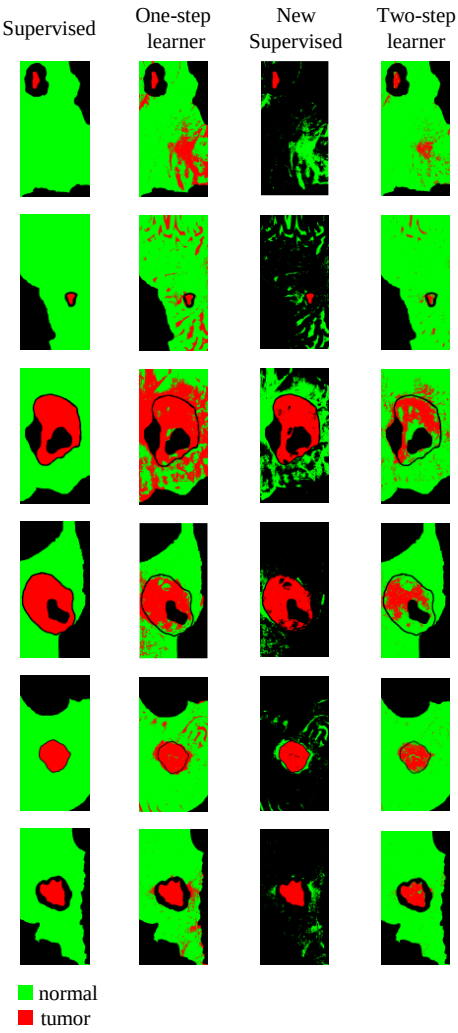

Fig. 4 Summary of images for comparison between the case with one learner and the case with two learners. From left to right: supervised image, results of the one-step learner, new supervised image, and results of the two-step learner.

machine that can also classify unexposed and necrotic tumor tissues, which were ignored in this study. We would also like to study image processing that can indicate gastric cancer by drawing a line around it.

For developing a practical diagnostic support system, it is necessary to sufficiently standardize individual differences. This problem might be resolved by increasing data preprocessing methods and data volume.

REFERENCES

[1] H. Sung, J. Ferlay, R. L. Siege, M. Laversanne, I. Soerjomataram et al., "Global Cancer Statistics 2020: GLOBOCAN Estimates of Incidence and Mortality Worldwide for 36 Cancers in 185 Countries," CA CANCER J CLIN., vol. 71, no.3, 2021, pp. 209-249.

[2] H. Katai, T. Ishikawa, K. Akazawa, Y. Isobe, I. Miyashiro et al., "Five-year survival analysis of surgically resected gastric cancer cases in Japan: a retrospective analysis of more than 100,000 patients from the nationwide registry of the Japanese Gastric Cancer Association (2001-2007)," Gastric Cancer, vol. 21, 2018, pp. 144–154.

[3] R. Miyahara, Y. Niwa T. Matsuura, O. Maeda, T. Ando et al., "Prevalence and prognosis of gastric cancer detected by screening in a large Japanese population: Data from a single institute over 30 years," Journal of Gastroenterology and Hepatology, vol. 22, no. 9, 2007, pp. 1435-1442.

[4] W. K. Leung, M. S. Wu, Y. Kakugawa, J. J. Kim, K. Yeoh et al., "Screening for gastric cancer in Asia: current evidence and practice," Lancet Oncol., vol. 9, no. 3, 2008, pp. 279-287.

[5] A. M. Smith, M.C. Mancini and S. Nie., "Second window for in vivo imaging," Nat. Nanotechnol., vol. 4, 2009, pp. 710–711.

[6] F. F. Jöbsis, "Noninvasive, infrared monitoring of cerebral and myocardial oxygen sufficiency and circulatory parameters," Science, vol. 198, no. 4323, 1997, pp. 1264-1267 .

[7] A. F. Goetz, G. Vane, J. E. Solomon and B. N. Rock, "Imaging spectrometry for Earth remote sensing," Science, vol. 228, 1985, pp. 1147–1153.

[8] O. Carrasco, R. B. Gomez, A. Chainani and W. E. Roper, "Hyperspectral imaging applied to medical diagnoses and food safety," Proc. SPIE, vol. 5097, 2003, pp. 215-221 .

[9] S. Kiyotoki, J. Nishikawa, T. Okamoto, K. Hamabe, M. Saito et al., "New method for detection of gastric cancer by hyperspectral imaging: a pilot study," J. Biomed. Opt., vol. 18, no. 2, 2013, 026010.

[10] H. Akbari, K. Uto, Y. Kosugi, K. Kojima, and N. Tanaka, "Cancer detection using infrared hyperspectral imaging," Cancer Sci., vol. 102, no. 4, 2011, pp. 852-857.

[11] D. Sato, T. Takamatsu, M. Umezawa, Y. Kitagawa, K. Maeda et al., "Distinction of surgically resected

gastrointestinal stromal tumor by near-infrared hyperspectral imaging," Sci. Rep., vol. 10, 2020, 21852.

[12] K. Akimoto, R. Ike, K. Maeda, N. Hosokawa, T. Takamatsu et al., "Wavelength Bands Reduction Method in Near-Infrared Hyperspectral Image based on Deep Neural Network for Tumor Lesion Classification," European Journal of Applied Sciences, vol. 9, no. 1, 2021, pp. 273–281.

[13] R. Tibshirani, "Regression Shrinkage and Selection via the Lasso," J. R. Stat. Soc., Series B, vol. 58, no. 1, 1996, pp. 267-288.

[14] R. Muthukrishnan, and R. Rohini, "LASSO: A feature selection technique in predictive modeling for machine learning," Conference: 2016 IEEE International Conference on Advances in Computer Applications (ICACA), 2016, pp. 18-20

[15] J.A. Gualtieri, and S. Chettri, "Support vector machines for classification of hyperspectral data," in Proc. IGARSS, Honolulu, HI, USA, 2000, pp. 813–815.

[16] Y. Langeron, M. Doussot, D. J. Hewson and J. Duchêne, "Classifying NIR spectra of textile products with kernel methods," Engineering Applications of Artificial Intelligence, vol. 20, no. 3, 2007, pp. 415-427.